AIP | Applied Physics Letters

Multi-perspective scanning microscope based on Talbot effect

Yangyang Sun and Shuo Pang

Citation: Applied Physics Letters **108**, 021102 (2016); doi: 10.1063/1.4939873
View online: http://dx.doi.org/10.1063/1.4939873
View Table of Contents: http://scitation.aip.org/content/aip/journal/apl/108/2?ver=pdfcov
Published by the AIP Publishing

Multi-perspective scanning microscope based on Talbot effect

Yangyang Sun and Shuo Pang[a)]
CREOL, College of Optics and Photonics, University of Central Florida, Orlando, Florida 32816, USA

(Received 18 September 2015; accepted 1 January 2016; published online 11 January 2016)

We report a multi-perspective scanning microscope based on the Talbot effect of a periodic focal spot array. Talbot illumination decouples the lateral scanning and the focal spots tuning. Large field of view fluorescence Talbot Microscope has been demonstrated by globally changing the incident wavefront gradient. Here, we explore the design freedom of adjusting the wavefront locally within each period and thus engineer the point spread function of the focal spots. We demonstrate an imaging system capable of reconstructing multi-perspective microscopic images in both bright field and fluorescence mode. With the multi-perspective imaging capability, we envision a more robust microscopic imaging system for large field of view fluorescence microscopy applications. This method is also suitable for compact imaging systems for multi-layer microfluidic systems. © *2016 AIP Publishing LLC*. [http://dx.doi.org/10.1063/1.4939873]

Since its first discovery[1] and explanation by Lord Rayleigh in diffraction theory,[2] self-imaging phenomena of periodic structures, known as the Talbot effect, have been extensively investigated under various circumstances[3,4] and in different wavelength regimes. Applications of the Talbot effect have been explored in precision metrology,[5,6] spectroscopy,[7] illumination design,[8,9] and x-ray phase imaging.[10] Recently, the self-imaging effect has been demonstrated in large field of view fluorescence microscopy, termed Fluorescence Talbot Microscope.[11] Different from other scanning microscope setup where the sample is directly scanned by the focal spots of a MicroLens Array (MLA),[12] Fluorescence Talbot Microscope scans the sample at Talbot distance away from the original focal spots, resulting in a longer working distance and an improved intensity uniformity of the focal spots. More importantly, the phase sensitivity of the Talbot effect decouples the scanning of the focal spot array and the modification of the intensity profile of individual focal spot. By generating a slight gradient to the global incident wavefront in the Fluorescence Talbot Microscope setup, we can scan the spot array for a significant distance without introducing off-axis aberrations, as illustrated in Fig. 1(a).

Different from changing the global wavefront gradient, changing the wavefront locally within each period provides another degree of freedom of design to engineer the point spread function of the focal spots, which can improve the performance of the scanning microscope. Hulskin *et al*. optimized the local wavefront to compensate for the higher order propagation phase term and achieved a high resolution Talbot focal spots array.[13] The application is also focused on large field of view microscopic imaging. In fact, for large field of view microscopy applications, calibration and alignment are major challenges: a small tilt of the sample plane or microlens array can lead to a substantial defocus of the image. Here, we demonstrate a method to generate Talbot images in multiple perspectives by changing the local wavefront. With multi-perspective views of the sample, we could numerically compensate the defocusing through post-processing, which is similar to the concept of plenoptical microscope,[14] and thus leads to a more robust large field of view system.

Talbot effect, in essence, is a two-dimensional periodic wavefront repeating itself periodically along the wave propagation direction. This period in the propagation direction is called the Talbot distance, D_T

$$D_T = \frac{2d^2}{\lambda}, \tag{1}$$

where d is the period of the wavefront, and λ is the wavelength of the light. In the setups where the period is $\sim 100\,\mu$m and wavelength is $\sim 0.5\,\mu$m, the working distance is ~ 40 mm, which is greater than the working distance of a scanning microscopy with an objective with similar Numerical Aperture (NA). With a conventional microscope objective, changing the wavefront gradient at the back focal plane shifts the imaging perspective and the field of view simultaneously. As mentioned earlier, in Talbot illumination set-up, we can adjust the global and local wavefront separately to scan the focal spots and change the imaging perspective, respectively. As shown in Fig. 1(b), the local wavefront can be adjusted by selectively illuminating the different regions of individual microlens. Shifting the illumination in the Fourier plane generates a "tilt" of the focal spots, which is equivalent to a shift in the scanning image perspective.

Our setup is based on the Talbot microscope system described previously[15] and is shown in Fig. 1(c). The microlens array (SUSS MicroOptics) has a pitch of 100 μm, and each microlens has a numerical aperture of 0.17. The local wavefront is changed by shifting a binary transmission aperture mask (HTA photomask) mounted on a motorized translation stage (LHA-HS, Newport). The Talbot image of the aperture mask is optically relayed to the microlens array. The diameter of individual aperture on the mask is 50 μm, and the period of the aperture array is 100 μm, matching that of the microlens array. The aperture size of the mask can be selected according to applications: smaller aperture diameter increases the focal depth and provides higher angular resolution, but with compromise in spatial resolution.

a)Electronic mail: pang@creol.ucf.edu.

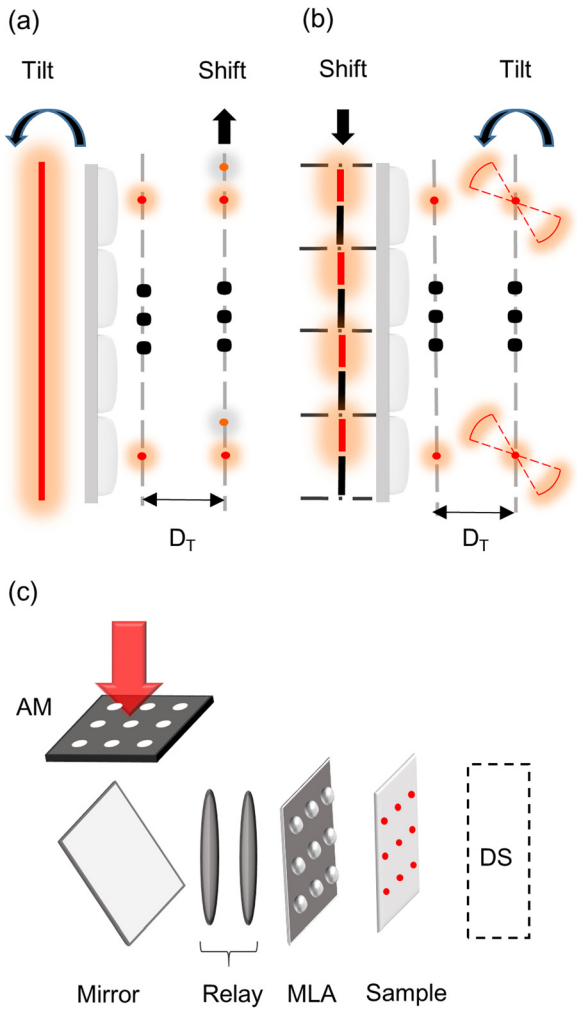

FIG. 1. (a) Changing the global wavefront. Red line denotes the original wavefront. A tilt of the global wavefront leads to a shift of the Talbot spots to scan the sample. (b) Changing the local wavefront. The local wavefront is changed by shifting an aperture mask to selectively illuminate individual microlens. The shift of the aperture mask leads to a tilt of individual Talbot focal spot. (c) Schematic of the system setup. AM: Aperture Mask. MLA: MicroLens Array. DS: Detection System. The piezo-driven mirror is placed at one Talbot distance from the AM. The Talbot image of the AM is relayed to the back plane of the MLA. The sample is placed at half Talbot distance from the MLA. An emission filter was added in the DS for fluorescence imaging.

This trade-off is similar to that of the light field microscopy.[14] We use a 488 nm laser (OBIS, Coherent) as the source. The sample is placed at half Talbot distance, 20.5 mm, from the focal plane of the microlens array. To scan the sample, the global wavefront is adjusted by a piezo-driven mirror (AG-M100L, Newport). The detection system consists of an objective (4X, NA = 0.13, Nikon), a tube lens (f = 150 mm, Newport), and a camera (Manta G-145B, AVT). It is worth noting that the spatial resolution of the system is determined by the illumination from the microlens array, and thus the objective in the detection system does not necessarily limit the field of view. Here, the field of view is 1.69 mm by 1.43 mm. A field of view as large as 15 mm has been demonstrated previously.[15] The sample is a two-layer patterned photoresist. SU-8 (MicroChem) is patterned on both side of a microscope cover slip. The height of the pattern is 15 μm, and the thickness of the cover slip are 155 μm. The pattern of the sample is an array of cylinders, each having 20 μm diameter, and the period of the pattern is 40 μm. The bright field image of the sample is shown in Fig. 2(a) by a conventional microscope objective (10X, NA = 0.3, Nikon).

Talbot Microscope images the sample from 5 successive perspectives by translating the aperture mask. The translation step size is 12 μm. The reconstructed images of these five perspectives of the two-layer sample are shown in Figs. 2(c1)–2(c5). The dark boundaries of the cylinders can be clearly observed due to the scattering at the edges. The total shift of the relative location of patterns on two layers is 11.1 μm.

We further quantify the spatial resolution and the focal depth of the multi-perspective Talbot Microscope. The spatial resolution is measured by imaging a USAF resolution target, the reconstructed image is shown in Fig. 3(a1). The discernable line width is 2.2 μm, as shown in Fig. 3(a2), and the profile of the pattern is shown in Fig. 3(a3), with a visibility of 0.24. We also measure the focal depth of the grid by scanning the focal spots along the axial direction by a microscope objective (20X, NA = 0.45, Nikon). The scanning step size is 25 μm. The intensity profile of the grid spot, shown as red line in Fig. 3(b), is compared with the simulation result in blue. The full width at half maximum (FWHM) of the

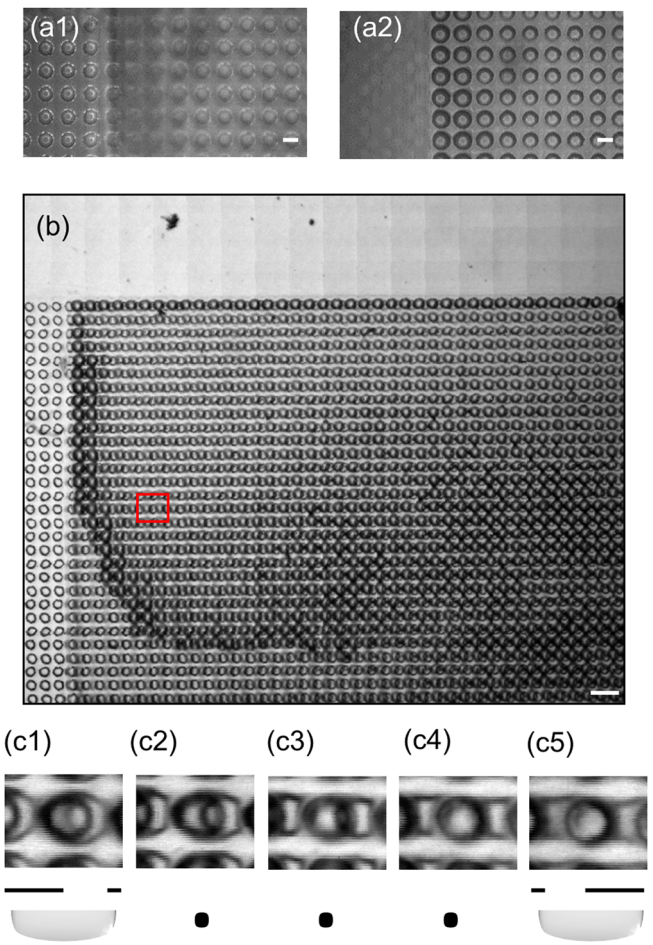

FIG. 2. (a1) and (a2) Images of the two-layer SU-8 sample with a conventional 10× microscope focusing on different layers. The scale bar is 20 μm. (b) The reconstructed image of the sample in 0°. The scale bar is 80 μm. (c1)–(c5) Reconstructed images in the red square of (b) from 5 perspectives. The aperture mask step size is 12 μm between adjacent perspectives.

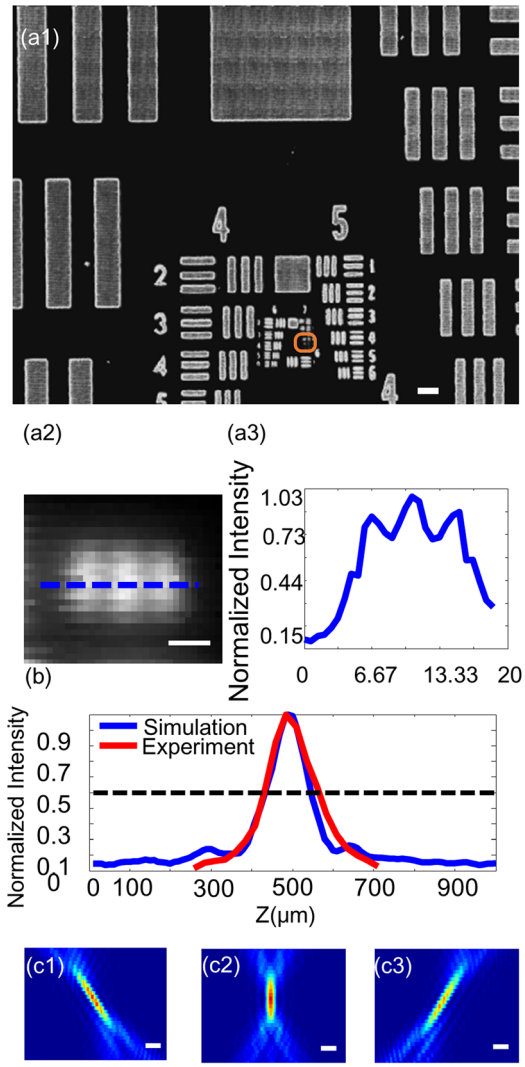

FIG. 3. (a1) The reconstructed image of the USAF resolution target. The scale bar is 300 μm. (a2) The image of the pattern with 2.2 μm line width. The scale bar is 5 μm. (a3) The profile of the intensity along the blue line in (a2). (b) The simulated intensity profile along the focal depth compared with the experimental measurements. (c1)–(c3) Simulated local point spread functions in air with Fourier plane aperture at -24 μm, 0, and 24 μm, respectively. The scale bar is 5 μm.

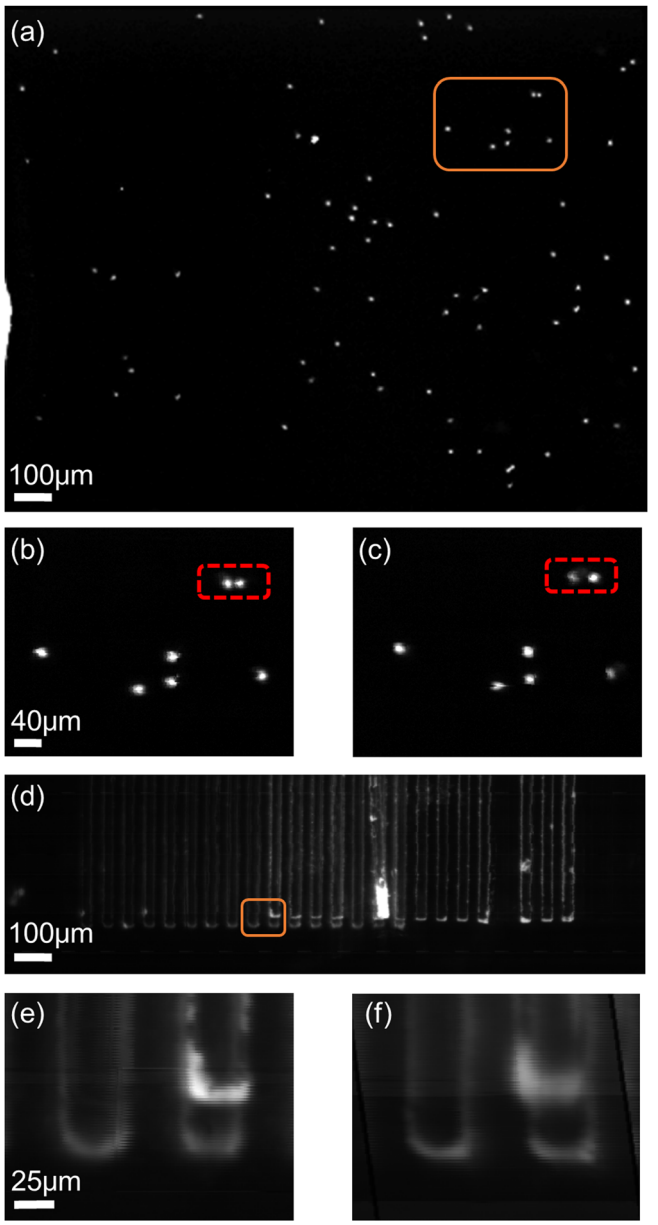

FIG. 4. (a) Reconstructed image of a two-layer fluorescent beads. (b) and (c) The magnified images of the beads in yellow square in (a) from two perspectives. The beads within the red box are located on different layers. (d) Reconstructed image of a two-layer fluorescent microfluidic channels. (e) and (f) Magnified images of the channels within the box in (d) from two perspectives.

experimental profile is 133 μm, and the simulated FWHM is 118 μm. The point spread functions with the aperture placed at the -24 μm, 0, and 24 μm from the center of the microlens are also simulated, as shown in Figs. 3(c1), 3(c2), and 3(c3), respectively. The angular perspective shift is 4.9°. For the two layers that are 155 μm apart, the relative shift is calculated to be 16.5 μm, which is comparable with the experimental measurement of 11.4 μm. The difference could be caused by the inaccuracy of the focal length of the microlens and the thickness of the coverslip.

We also demonstrate the capability of the system operating in the fluorescence mode. The fluorescent sample is a two-layer sample of air dried fluorescent beads ($d = 15$ μm, FS07F, Bangs Laboratories) on both side of a cover slip. The scanning step size is 0.63 μm. The dwell time of each step is 0.138 s. We have inserted a fluorescence filter (D535/40, Chroma) in the detection path. The full field of view image from the perspective of 4.9° is shown in Fig. 4(a). Figs. 4(b) and 4(c) show a magnified region viewed from 4.9° and -4.9° angular perspectives. The area highlighted by the red box shows two beads from different layers, and the relative distance of the beads changes in different perspectives. We also checked the sample in conventional microscope and verified that the two beads were located on different layers. The change of the distance between two beads is 11.25 μm. Since the point spread functions are modified on the illumination side, the fluorescence collection efficiency is not affected by changing the perspective. In complex microfluidic systems, multiple layers can be distinguished from multi-perspective views with long imaging depth and could thus eliminate the adjustment of focus. Here, we perform a two-perspective fluorescence imaging of a two-layer microfluidic channels. The vertical separation of the two layers is

170 μm, and the width of the microfluidic channels is 28 μm. The quantum dots solutions (753769, Aldrich) are dried on the bottom and side walls of each channel, giving the fluorescence light. The reconstructed images are shown in Figs. 4(d)–4(f). The lateral shift of two channels is 11.3 μm from different perspectives. Here, we would like to mention the difference between our system and integral imaging[14,16] which also generates multi-perspective images using microlens array. The depth resolution of the reconstructed 3D image is limited by the angular range from different perspectives. The angular range of our method is limited by the NA of individual microlens, while the angular range of integral imaging is limited by the extent of the MLA or the objective lens. Given the NA = 0.17 of the microlens, our setup could achieve a depth resolution of 12.7 μm.

In summary, we have demonstrated a scalable field of view multi-perspective microscope that can operate in both bright field and fluorescence mode. Different from a conventional scanning microscope, the Talbot Microscope decouples the lateral scanning Talbot spot and the focal spots tuning. The multi-perspective imaging can be achieved by adjusting the local wavefront. We expect further development based on the concept of engineering the point spread function of the Talbot illumination. With the long focal depth and multi-perspective imaging capability, we envision a more robust large field of view fluorescence imaging system. The demonstrated method is also suitable for a compact imaging system for multi-layer microfluidic system.

The authors would like to thank Professor Changhuei Yang at Caltech for the support in the experimental setup and Zhuyuan Zhu at CREOL for his help in the experiment.

[1]H. F. Talbot, Philos. Mag. Ser. 3 **9**, 401 (1836).
[2]Lord Rayleigh, Philos. Mag. Ser. **11**, 196 (1881).
[3]C. Zhou, S. Stankovic, and T. Tschudi, Appl. Opt. **38**, 284 (1999).
[4]M. Paturzo, F. Merola, and P. Ferraro, Opt. Lett. **35**, 1010 (2010).
[5]D. S. Mehta, S. K. Dubey, C. Shakher, and M. Takeda, Appl. Opt. **45**, 7602 (2006).
[6]H. Luo, C. Zhou, H. Zou, and Y. Lu, Opt. Commun. **248**, 97 (2005).
[7]S. De Nicola, P. Ferraro, G. Coppola, A. Finizio, G. Pierattini, and S. Grilli, Opt. Lett. **29**, 104 (2004).
[8]A. W. Lohmann and J. A. Thomas, Appl. Opt. **29**, 4337 (1990).
[9]Y. Luo, V. R. Singh, D. Bhattacharya, E. Y. S. Yew, J.-C. Tsai, S.-L. Yu, H.-H. Chen, J.-M. Wong, P. Matsudaira, P. T. C. So, and G. Barbastathis, Laser Photonics Rev. **8**, L71 (2014).
[10]A. Momose, S. Kawamoto, I. Koyama, Y. Hamaishi, K. Takai, and Y. Suzuki, Jpn. J. Appl. Phys. **42**, 7B (2003).
[11]S. Pang, C. Han, M. Kato, P. Sternberg, and C. Yang, Opt. Lett. **37**, 5018 (2012).
[12]A. Orth and K. Crozier, Opt. Express **20**, 13522 (2012).
[13]B. Hulsken, D. Vossen, and S. Stallinga, J. Eur. Opt. Soc. - Rapid Publ. **7**, 12026 (2012).
[14]M. Levoy, R. Ng, A. Adams, M. Footer, and M. Horowitz, ACM Trans. Graphics **25**, 924 (2006).
[15]S. Pang, C. Han, J. Erath, A. Rodriguez, and C. Yang, Opt. Express **21**, 14555 (2013).
[16]S.-H. Hong, J.-S. Jang, and B. Javidi, Opt. Express **12**, 483 (2004).